Nanoscale

PAPER

View Article Online
View Journal | View Issue

Cite this: *Nanoscale*, 2021, **13**, 15952

Cucurbit[6]uril@MIL-101-Cl: loading polar porous cages in mesoporous stable host for enhanced SO_2 adsorption at low pressures†

Yangyang Sun, [a] Jun Liang, [a,b] Philipp Brandt, [a] Alex Spieß, [a] Secil Öztürk [a] and Christoph Janiak *[a,b]

The robust cucurbituril-MOF composite CB6@MIL-101-Cl was synthesized by a wet impregnation method and a concomitant OH-to-Cl ligand exchange {CB6 = cucurbit[6]uril, 31 wt% content in the composite, MIL-101-Cl = $[Cr_3(O)Cl(H_2O)_2(BDC)_3]$, BDC = benzene-1,4-dicarboxylate}. MIL-101-Cl was formed postsynthetically from standard fluorine-free MIL-101 where Cr-OH ligands were substituted by Cl during treatment with HCl. CB6@MIL-101-Cl combines the strong SO_2 affinity of the rigid CB6 macrocycles and the high SO_2 uptake capacity of MIL-101, and shows a high SO_2 uptake of 438 cm^3 g^{-1} (19.5 mmol g^{-1}) at 1 bar and 293 K (380 cm^3 g^{-1}, 17.0 mmol g^{-1} at 1 bar and 298 K). The captured SO_2 amount is 2.2 mmol g^{-1} for CB6@MIL-101-Cl at 0.01 bar and 293 K (2.0 mmol g^{-1} at 298 K), which is three times higher than that of the parent MIL-101 (0.7 mmol g^{-1}) under the same conditions. The near zero-coverage SO_2 adsorption enthalpies of MIL-101 and CB6@MIL-101-Cl are −35 kJ mol^{-1} and −50 kJ mol^{-1}, respectively, reflecting the impact of the incorporated CB6 macrocycles, having higher affinity towards SO_2. FT-IR spectroscopy confirms the interactions of the SO_2 with the cucurbit[6]uril moieties of the CB6@MIL-101-Cl composite and SO_2 retention for a few minutes under ambient air. Comparative experiments demonstrated loss of crystallinity and porosity after dry SO_2 adsorption for MIL-101, while CB6@MIL-101-Cl exhibits nearly complete retention of crystallinity and porosity under the exposure to both dry and wet SO_2. Thus, CB6@MIL-101-Cl can be an attractive adsorbent for SO_2 capture because of its excellent recycling stability, high capacity and strong affinity toward SO_2 at low pressure.

Received 8th July 2021,
Accepted 7th September 2021

DOI: 10.1039/d1nr04432j

rsc.li/nanoscale

Introduction

The large-scale emission of flue gases containing toxic SO_2 arouses increasing worldwide concerns. As of 2010, global energy sector emissions of SO_2 were estimated to be about 40 Tg.[1] The majority of anthropogenic SO_2 emissions originated from coal- and oil-burning for electricity generation.[2] SO_2 is responsible for human respiratory diseases including bronchitis, asthma as well as cardiovascular diseases,[3,4] and SO_2 along with NO_X emissions lead to the formation of 'acid rain' that poses significant danger to the health of ecosystems, particularly by inhibiting plant growth and poisoning aquatic life.[5] In addition, SO_2 can react with other air pollutants to produce sulphate particles, which are a main component of fine particulate matter ($PM_{2.5}$).[6,7] Thus, developing new materials and technologies for SO_2 removal is imperative.

Limestone scrubbing, ammonia scrubbing and absorptive removal by organic solvents like monoethanol–amine (MEA) represent the majority of conventional technologies of SO_2 removal from flue gases. A capture of more than 95% SO_2 from the gas mixtures could be achieved *via* use of these traditional approaches.[8–10] Improvements in energy efficiency and decrease of wastes suggest physisorption by solid adsorbents as the most promising alternatives, particularly due to the possibility to minimize energy requirements. It is worth noting that because of the corrosive nature of SO_2, its complete as possible removal as the first step of flue gas processing allows broader possibilities for subsequent purification/sequestration steps.[11,12] Therefore, the development of chemically resistant porous materials for adsorptive SO_2 removal, especially with high uptake and selectivity at industrially relevant low partial pressures of SO_2, is of great interest.

[a]*Institut für Anorganische Chemie und Strukturchemie, Heinrich-Heine-Universität Düsseldorf, 40204 Düsseldorf, Germany. E-mail: janiak@hhu.de*
[b]*Hoffmann Institute of Advanced Materials, Shenzhen Polytechnic, 7098 Liuxian Blvd, Nanshan District, Shenzhen 518055, China*

†Electronic supplementary information (ESI) available: Elemental analysis for CB6@MIL-101-Cl, setup for humid SO_2 exposure experiments, PXRD, FT-IR, SEM, EDX and XPS analysis, details for SO_2 sorption isotherm fitting, comparison of SO_2 sorption for MOFs, isosteric enthalpy of adsorption, 3 cycles of full SO_2 adsorption–desorption measurement, PXRD after cyclic measurement and exposure to humid SO_2, SO_2 adsorption isotherms after exposure to humid SO_2. See DOI: 10.1039/d1nr04432j

Metal–organic frameworks (MOFs) have drawn intensive attention in the context of gas storage and separation.[13–15] Due to their high surface area, high pore volume and tunable surface functionality, MOFs can be designed for sorption of toxic chemicals including SO_2,[16–19] and the capture of CO_2.[20] The stability of MOFs against water vapors should not be overlooked during evaluation of potential MOF adsorbents for SO_2 capture.[21] Although some MOFs have been reported to be promising for SO_2 adsorption and SO_2/CO_2 separation,[22–30] the efficient MOF-based adsorbents with both high stability and high-capacity are still very limited.

MIL-101(Cr), which possesses excellent water stability, high surface area and micro/mesoporosity (29 and 34 Å inner diameter), is a particularly interesting adsorbent for practical applications (the guest-free form corresponds to $[Cr_3(\mu_3\text{-}O)(X)(H_2O)_2(BDC)_3]$, X = F, OH, BDC = benzene-1,4-dicarboxylate). In 2020, Ibarra *et al.* reported that MIL-101(Cr)-4F(1%) (−4F = fully fluorinated BDC) shows a high SO_2 uptake capacity of 18.4 mmol g^{-1} at 1 bar and 298 K and is chemically stable towards dry and humid SO_2.[31] The large pore volume, beneficial at higher pressures, is the primary reason for the superior performance of MIL-101(Cr) at 1 bar compared to other microporous MOFs. However, MIL-101(Cr) shows mediocre uptake at low pressure due to the lower density of strongly adsorbing sites, such as open-metal sites,[32] and polar OH^- and H_2O ligands. MIL-101(Cr) has also no polar ligand substituents, such as $-NH_2$ or –OH groups and lacks small micropores in the 4–8 Å region, both of which are advantageous for a low-pressure uptake of SO_2.[25,33–35] Importantly, it was also shown that the MIL-101(Cr) (formed by standard fluorine-free conditions), would gradually lose its crystallinity and, therefore the accessible surface area after SO_2 sorption at 298 K even under nearly anhydrous conditions.[31]

One effective method to modulate the pore size of a host framework is to introduce functional molecules to obtain composite materials, which may exhibit synergetic performances towards certain adsorbates.[36–40] However, MOF-based composites are not yet reported for SO_2 sorption and separation until now to the best of our knowledge. Recently, our group studied the outstanding SO_2 sorption and separation performance of a cucurbit[6]uril microporous hydrogen-bonded organic framework (HOF),[41] nanoCB6-H (H stands for the solid-state honeycomb-like structure).[42,43] It was found that the CB6 cages ("barrels") have strong interactions with dry SO_2 molecules by forming interactions both on the outer surfaces and in its intrinsic pores at a low pressure.[41] However, the exposure of this CB6 HOF material to humid SO_2 conditions led to a phase change and major loss of porosity (particularly its extrinsic pores) due to its weak hydrogen bonds. We propose that the shortcomings of CB6 HOF frameworks can be circumvented by dispersing CB6 molecules in a MOF matrix such as MIL-101 to obtain CB6@MIL-101 (Scheme 1).[44] Herein, we report the preparation and characterizations of the targeted CB6@MIL-101-Cl material, which show enhanced SO_2 sorption behavior due to the combined merits of high host surface area, optimized pore sizes, CB6 molecules with high SO_2 affinity and increased stability toward SO_2 molecules. Since CB6 molecules are confined in the pores of MIL-101 frameworks, the performance is less affected by moisture or humid SO_2. Further, we discovered that hydrochloride could modify the MIL-101 framework and enhance the stability of the resultant CB6@MIL-101-Cl material toward corrosive SO_2 molecules. This work demonstrates for the first time the potential of cage@MOF composite materials for enhanced SO_2 removal and storage at low pressures.

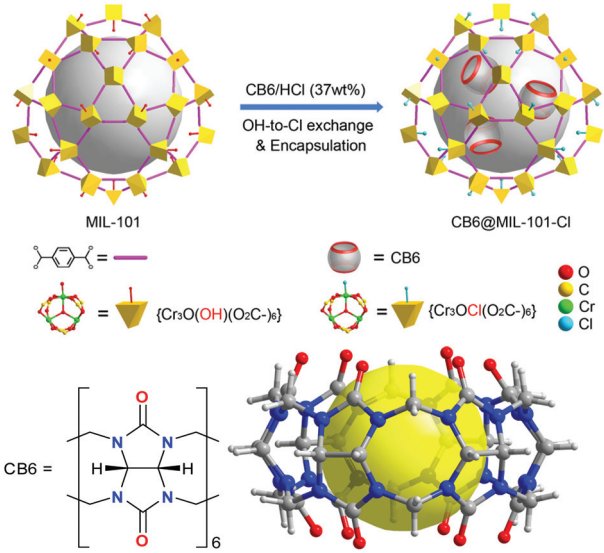

Scheme 1 Top: Schematic representation of the encapsulation of CB6 molecules in MIL-101 with the formation of the CB6@MIL-101-Cl composite. The two coordinated aqua ligands on the trinuclear chromium SBU are not indicated for clarity. Bottom: Formula and structure of CB6 = cucurbit[6]uril. The yellow sphere represents the intrinsic pore.

Experimental

Materials

All starting materials and solvents were obtained from commercial sources and used as delivered (Table S1†). CB6 was synthesized according to the literature.[44]

Characterization methods

Powder X-ray diffraction (PXRD) data were collected at room temperature on Rigaku Miniflex 600 powder diffractometer using a low background silicon sample holder and Cu-Kα radiation (λ = 1.5418 Å). The measurements were performed over a 2θ = 2–50° range with a scan speed of 1.5 deg min^{-1} (600 W, 40 kV, 15 mA). The diffractograms were analysed using the software Match!.[45]

Elemental analysis (CHNS) was carried out using an Elementar Analysensysteme vario MICRO cube instrument. The samples were dried at 150 °C under a vacuum for at least 20 h prior to the measurement.

Fourier transform infrared (FT-IR) spectra were measured on a Bruker FT-IR Tensor 37 spectrometer at room temperature

in the range of 550–4000 cm^{-1} using an attenuated total reflection (ATR) technique (Platinum ATR-QL, diamond). The activated samples were exposed to dry SO_2 for 15–30 minutes at room temperature (samples were activated prior to the procedure at 150 °C for 20 h). Then the sealed sample tubes with the MOF in SO_2 atmosphere were stored at 77 K for the transfer to the FT-IR instrument room. The tube was allowed to heat up to ~273 K and a sample was quickly transferred onto the crystal of the ATR unit, and the stamp of the ATR-unit was immediately closed afterwards. The change of the SO_2 amount in the sample was monitored during up to 10 minutes (note that the goal of the experiment was to qualitatively monitor the spectral changes). Resolution: 2 cm^{-1}; Sampling time: 16 scans; Background measuring time: 16 scans.

Scanning electron microscopy (SEM) was performed using a Jeol JSM-6510LV QSEM Advanced electron microscope with a LaB_6 cathode operating at 20 keV. The microscope was equipped with a Bruker Xflash 410 silicon drift detector for energy-dispersive X-ray (EDX) spectroscopy.

The nitrogen adsorption isotherms were collected at 77 K on a Quantachrome Autosorb-6 automatic adsorption analyzer and evaluated with the AsiQwin V3 software. The samples were degassed in 10^{-2} mbar vacuum at 150 °C prior to the measurement. The Brunauer–Emmett–Teller (BET) surface areas were calculated using the data in the p/p_0 range of 0.05–0.2. The total pore volumes were calculated from the adsorbed volume corresponding to $p/p_0 = 0.90$. All gas uptake volume for N_2 and SO_2 is given at standard temperature and pressure, STP, *i.e.* the equivalent volume at 273.15 K and 1.013 bar.

The SO_2 sorption isotherms were collected at 273 K and 293 K on a Quantachrome Autosorb iQ MP instrument in 1×10^{-3}–1 bar pressure range. All samples were activated for at least 12 hours at 150 °C and <0.01 mbar vacuum prior to each experiment.

The cyclic SO_2 sorption experiments were carried out on a Quantachrome Autosorb iQ MP at 293 K. For the three-cycle ad/desorption measurements, full isotherms (with 17 points for ads. and 12 points for des.) were collected for MIL-101, MIL-101-Cl and CB6@MIL-101-Cl. Between each individual isotherm sorption experiment the samples were activated at 150 °C under vacuum (1×10^{-3} mbar) for 12 hours. For the 10-cycle adsorption measurements for CB6@MIL-101-Cl, three points (at 0.01, 0.5 and 0.96 bar) were set for quick analysis of adsorption and desorption and also with activation at 150 °C under vacuum (1×10^{-3} mbar) for 30 minutes before the next cycle was started.

X-ray photoelectron spectroscopy (XPS) was conducted on a ULVAC-PHI VersaProbe II microfocus X-ray photoelectron spectrometer. The spectra were recorded using a polychromatic aluminium Kα X-ray source (1486.8 eV) and referenced to the carbon 1s orbital with a binding energy of 284.8 eV. Experimental XP spectra were fitted by the CasaXPS Software (version 2.3.19PR1.0).

Syntheses

MIL-101. The synthesis was carried out according to a literature method.[46] Chromium(III) nitrate nonahydrate ($Cr(NO_3)_3 \cdot 9H_2O$; 1.920 g, 4.8 mmol), benzene-1,4-dicarboxylic acid, (H_2BDC; 0.813 g, 4.9 mmol), deionized water (24 mL) and nitric acid (HNO_3; 0.475 g, 4.9 mmol) as modulator were added in the given sequence. The mixture was stirred for half an hour, and the formed slurry was accurately transferred to a PTFE insert of a hydrothermal autoclave. The sealed autoclave was heated at 200 °C for 15 h. After cooling, the obtained solid was separated and washed by dimethylformamide (DMF; 2 × 50 mL) and ethanol (EtOH; 3 × 50 mL) *via* centrifugation. The product was dried at 65 °C overnight. The activation of MIL-101 was performed by degassing at 150 °C and ≤0.01 mbar vacuum for 20 hours.

CB6@MIL-101-Cl. The loading of CB6 to MIL-101 was performed *via* impregnation, according to a literature method.[44] 100 mg of MIL-101 was pre-activated and then added to a solution of 50 mg cucurbit[6]uril (CB6) in 2 mL of concentrated HCl (37 wt%), prepared using sonication. The slurry of MIL-101 was stirred for 4 hours using a magnetic stirrer (strong stirring was avoided in order to preserve the morphology of the material). The resultant solid was washed first by 2 × 6 mL of HCl (37 wt%), followed by 2 × 20 mL of deionized water and finally 2 × 20 mL of 96% ethanol (all separations were performed *via* centrifugation). The obtained green solid was dried at 65 °C in an oven. The composition of the composite was assessed on its elemental analysis data and in line with previous work[44] as $[Cr_3(O)Cl(H_2O)_2(C_8H_4O_4)_3][C_{36}H_{36}N_{24}O_{12}]_{0.33}$ of 31 wt% of CB6 in CB6@MIL-101-Cl (see ESI† for details).

MIL-101-Cl. The activated MIL-101 (100 mg) was treated by HCl (37 wt%, 2 mL) exactly like described in the synthesis of CB6@MIL-101-Cl but without the addition of CB6.

NanoCB6-H. For comparison in SO_2 sorption, the preparation of nanoCB6-H was carried out according to the literature.[41] 250 mg of CB6 was dissolved in diluted HCl (5 mL, 6 mol L^{-1}) under sonication (~2 min). The solution was filtered using a syringe filter (0.2 μm) and poured into 25 mL of methanol under stirring. The formed milky solution was centrifuged for 5 minutes, and the precipitate was washed twice with methanol (25 mL each). Finally, the obtained solid was dried at 65 °C in oven and ground slightly for further use. For activation, nanoCB6-H was degassed at 150 °C for 48 hours.

Humid SO_2 stability test (performed on MIL-101, nanoCB6-H, and CB6@MIL-101-Cl)

The method closely follows the description in the literature (Scheme S1, ESI†).[25] A pre-dried air stream (2 L min^{-1}) was bubbled through an aqueous sodium metabisulfite solution (0.4 g $Na_2S_2O_5$ in 80 mL water) within a Schlenk flask (250 mL). The setup was equipped with a 3-way valve to regulate the outlet of the gas flow. The outlet of the flask was either connected to a desiccator, playing the role of a humidity chamber, or to the exhaust air when the concentration of SO_2 in the chamber reached the target value. The diluted SO_2 stream flowed through the desiccator and escaped through a vent. The desiccator contained a crystallizing dish filled with saturated sodium chloride solution (80 mL) ensuring a relative

humidity (RH) near 75%. The RH value was monitored with a VWR TH300 hygrometer and the SO_2 content with Dräger Pac 6000 electrochemical sensor.

50 mg of each MIL-101, nanoCB6-H and CB6@MIL-101-Cl were pre-activated (≤0.01 mbar, 150 °C overnight) and exposed to humid SO_2 (35 ± 5 ppm content in the gas stream) by placing them in the desiccator at 75% relative humidity in open broad-necked glass vials for 6 hours at room temperature. Afterwards, the samples were dried at 65 °C in the oven and activated (≤0.01 mbar, 150 °C overnight) for further measurements.

Results and discussion

MIL-101, chromium(III) terephthalate, is built of trinuclear $\{Cr_3(\mu_3\text{-}O)X(H_2O)_2(O_2C\text{-})_6\}$, X = F, OH secondary building units (SBUs), which are bridged by the terephthalate linkers (BDC^{2-}), forming a porous zeotypic framework with two types of mesocages with diameters of 29 and 34 Å.[47,48] The small cages have pentagonal windows with a diameter of 12 Å, and the large cages have hexagonal windows with diameters of 15 Å in addition to the pentagonal windows (Scheme S2, ESI†). The molecular size of CB6 is 14.4 Å with a height of 9.1 Å.[44] Depending on the synthetic conditions the trinuclear unit has either a charge-compensating fluorido or a hydroxido ligand coordinated by one of the chromium atoms of the SBU.

MIL-101, $[Cr_3(\mu_3\text{-}O)(OH)(H_2O)_2(BDC)_3]$ was prepared according to the literature,[44] and was used as a host to load CB6, which was performed *via* stirring of the MIL-101 in a CB6 solution in conc. HCl (37 wt%) (Scheme 1). We refer to this process as "wet impregnation". It should be noted that cucurbit[6]uril was dissolved in conc. HCl (37 wt%) before being treated with MIL-101. A composite material designated as CB6@MIL-101-Cl was the result of the loading of CB6 into MIL-101. The treatment of the MIL-101 host with the HCl solution caused the simultaneous exchange of the charge-balancing hydroxido ligand by chlorido ligand, transforming the host framework to MIL-101-Cl, $[Cr_3(\mu_3\text{-}O)Cl(H_2O)_2(BDC)_3]$ during the loading (Scheme 1). Thus, the formation of CB6@MIL-101-Cl, containing 31 wt% of CB6 according to the elemental analysis, and the conversion of the framework by exchange of the terminal anionic ligand, were performed as a concomitant "one-pot" process.

Powder X-ray diffraction (PXRD) confirmed the phase purity of MIL-101 and the retention of the MIL-101 framework structure in CB6@MIL-101-Cl (Fig. S1, ESI†). The nearly identical PXRD patterns confirmed that neither the hydroxido-to-chlorido exchange nor the encapsulation of CB6 into the pores influences the structure of the framework significantly. Compared with the Fourier transform infrared (FT-IR) spectroscopy of MIL-101, CB6@MIL-101-Cl shows additional peaks at 1740 cm^{-1} and at 1465 cm^{-1} due to the carbonyl and methylene groups of CB6 (Fig. S2, ESI†).[44]

The extent of the hydroxido-to-chlorido ligand exchange was quantified by energy dispersive X-Ray analysis (EDX) and X-ray photoelectron spectroscopy (XPS) measurements. For MIL-101 a negligible Cl content was confirmed by both EDX and XPS. EDX data (Fig. S3, Table S3, ESI†) suggests a $[Cr_3(\mu_3\text{-}O)Cl_x(OH)_{1-x}(H_2O)_2(BDC)_3]$ framework formula with x = 0.78 in the CB6@MIL-101-Cl composite. The Cl/Cr_3 ratio was checked also after one-cycle of SO_2 adsorption–desorption. As a result, the value x = 0.69 was found for CB6@MIL-101-Cl (Fig. S3, Table S3, ESI†), which are slightly lower compared to the initial materials, *i.e.*, prior to the SO_2 adsorption–desorption cycle, but still within experimental error.

XPS measurements were carried out after one-cycle of SO_2 adsorption–desorption (Fig. S4–S5, ESI†). The Cl/Cr_3 ratio or x in $[Cr_3(\mu_3\text{-}O)Cl_x(OH)_{1-x}(H_2O)_2(BDC)_3]$ was 1.08 in CB6@MIL-101-Cl (Table S4, ESI†). The XPS survey spectra show Cr and S for MIL-101, and Cr and Cl but no S for CB6@MIL-101-Cl (Fig. S4, ESI†). The S content in CB6@MIL-101-Cl was not detectable. The high-resolution Cl 2p spectrum for CB6@MIL-101-Cl features the Cl $2p_{1/2}$ and Cl $2p_{3/2}$ pair of peaks at 199.2 eV and 197.5 eV binding energies (Fig. S5, ESI†), which corresponds to a chloride ion,[49–51] in line with the spin–orbit splitting value of 1.6 eV. The high-resolution Cr 2p XPS spectrum exhibits peaks at 587.3 eV and 577.8 eV for MIL-101, and 586.7 eV and 577.3 eV for CB6@MIL-101-Cl (Fig. S5, ESI†). These values correspond well to typical 587.4 eV and 577.8 eV binding energies for Cr^{III} 2p (two Cr 2p peaks are observed due to spin–orbit splitting, which matches the expected value of 9.3 eV).[52–54] The 0.5–0.6 eV shift to lower binding energy of Cr 2p for CB6@MIL-101-Cl compared with MIL-101 derives from the slight change of the average Cr environment due to the hydroxido-to-chlorido exchange.

The high-resolution S 2p spectrum for MIL-101 (Fig. S5, ESI†) exhibits the S $2p_{1/2}$ and S $2p_{3/2}$ pair of peaks at 170 eV and 168.8 eV binding energies with a peak separation of 1.2 eV, which verified the chemical oxidation state of S(IV).[55] The S/Cr_3 ratio is 4.23 in MIL-101 after one-cycle of SO_2 adsorption–desorption (Table S4, ESI†). In contrast, sulfur could not be detected in CB6@MIL-101-Cl after SO_2 sorption. Since XPS operates under high vacuum we suggest putatively an initial reaction of Cr-OH in MIL-101 with SO_2 under formation of Cr-hydrogensulfite, Cr-OSO_2H or -disulfite, Cr-OS_2O_4H leading to an opening up of Cr coordination sites for further SO_2 chemisorption. The S 2p XPS spectrum of MIL-101 matches with metal(Ce, Ti)-sulfite/hydrogensulfite.[21,56,57]

Scanning electron microscopy (SEM) images further confirmed the retention of the morphology, thereby supporting the expected stability of the material also on the macroscopic level under mild adsorptive loading conditions. The synthesized MIL-101 and CB6@MIL-101-Cl phases have similar particle sizes (0.5–2.0 μm) and feature octahedral crystals typical for MIL-101.[58,59] (Fig. S6, ESI†). The absence of other significant crystal forms or coverage of the octahedral surfaces indicates that CB6 has not crystallized separately on the outer surface of the MIL-101 crystallites.

The porosity of the samples was assessed by analysis of the N_2 adsorption–desorption isotherms measured at 77 K. The

isotherm types of both MIL-101 and CB6@MIL-101-Cl are similar and retain the characteristic two-step shape (corresponds to IUPAC type Ib isotherms)[60] (Fig. 1). As expected, the uptake decreases after the encapsulation of CB6 in MIL-101. The Brunauer–Emmett–Teller (BET) surface areas for MIL-101 and CB6@MIL-101-Cl were found to be 3217 $m^2\ g^{-1}$ and 2077 $m^2\ g^{-1}$, respectively, their pore volumes 1.54 $cm^3\ g^{-1}$ and 1.00 $cm^3\ g^{-1}$ (assessed at p/p_0 = 0.9; Table S2, ESI†). The BET surface area for nanoCB6-H was 435 $m^2\ g^{-1}$.

The SO_2 adsorption–desorption isotherms were measured for MIL-101 and CB6@MIL-101-Cl at 293 K and 298 K and nanoCB6-H at 293 K (Fig. 2a). All three materials feature a relatively narrow hysteresis for the whole measured range. MIL-101 has an almost linear SO_2 uptake reaching 620 $cm^3\ g^{-1}$ and 584 $cm^3\ g^{-1}$ (27.7 mmol g^{-1} and 24.4 mmol g^{-1}) at 293 K and 298 K, respectively, and 1 bar. Expectedly, as the temperature increases, the amount of gas adsorbed decreases. On the other hand, the uptake for the nanoCB6-H is 6.5 mmol g^{-1} (145 $cm^3\ g^{-1}$) at 1 bar and 293 K, in line with its comparatively low total pore volume (Table S2, ESI†). However, about 43% of the total uptake of nanoCB6-H occurs in the low-pressure range of 0–0.01 bar, which reflects the strong affinity of CB6 toward SO_2 (Fig. 2b, Fig. S7, Table S5, ESI†). "Nano" in nanoB6-H refers to a particle size of 100–500 nm. NanoCB6-H shows a higher SO_2 uptake (63 $cm^3\ g^{-1}$, 145 $cm^3\ g^{-1}$) than micro-size crystallites of CB6 (43 $cm^3\ g^{-1}$, 98 $cm^3\ g^{-1}$) at both 0.01 bar and 0.97 bar and 293 K, due to the faster diffusion of SO_2 molecules in nanoCB6-H with smaller CB6 particle size.[41]

The CB6@MIL-101-Cl composite combined the merits of the two materials for SO_2 adsorption. It merges the strong affinity of the CB6 cages at low pressure and the high capacity of MIL-101. At 1 bar, a high SO_2 uptake of 438 $cm^3\ g^{-1}$ or 380 $cm^3\ g^{-1}$ (19.5 mmol g^{-1}, 17.0 mmol g^{-1}) at 293 K or 298 K, respectively, is reached, which is better than for most other SO_2-stable MOF materials (Table S6, ESI†), except of MIL-101 (27.7 mmol g^{-1} at 293 K), MOF-177 (25.7 mmol g^{-1} at 293 K)[29] and close to MFM-170 (17.5 mmol g^{-1} at 298 K).[24] However, MOF-177 and MIL-101 are unstable after SO_2 exposure, while the composite CB6@MIL-101-Cl is stable after SO_2 exposure. Understandably, the maximum uptake decreases somewhat in the CB6@MIL-101-Cl composite compared to the MIL-101 host, due to a lower total pore volume (Table S2, ESI†). The SO_2 adsorption isotherms of MIL-101 and CB6@MIL-101-Cl at 1 bar did not reach saturation as they still have a high positive slope and are far from levelling off. Saturation will require a pressure above 1 bar.

At 0.01 bar and 293 K the captured SO_2 amount was 2.2 mmol g^{-1} (2.0 mmol g^{-1} at 298 K) for CB6@MIL-101-Cl compared to 0.7 mmol g^{-1} (0.6 mmol g^{-1} at 298 K) for MIL-101, *i.e.*, a remarkable improvement by a factor of three (Fig. 2b). For comparison, the SO_2 uptake of nanoCB6-H was found to be 2.8 mmol g^{-1} at 0.01 bar. The important steep increase in the uptake of SO_2 by CB6@MIL-101-Cl in the low-pressure zone demonstrates the desirable efficiency for SO_2 removal at low partial pressure. The calculated mass-weighted SO_2 uptake for a physical mixture of CB6 and MIL-101 would

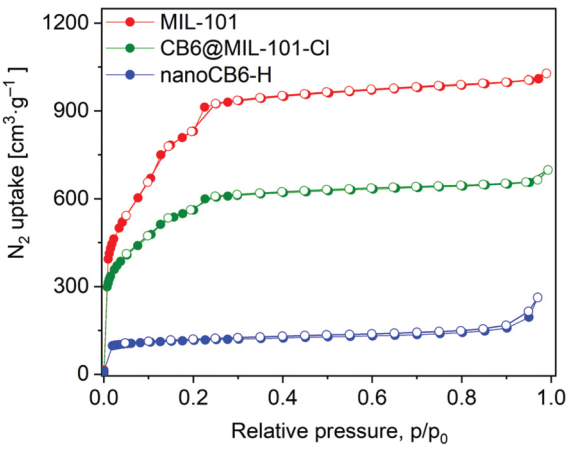

Fig. 1 Nitrogen adsorption–desorption isotherms at 77 K of MIL-101, CB6@MIL-101-Cl and nanoCB6-H. Filled symbols, adsorption; empty symbols, desorption.

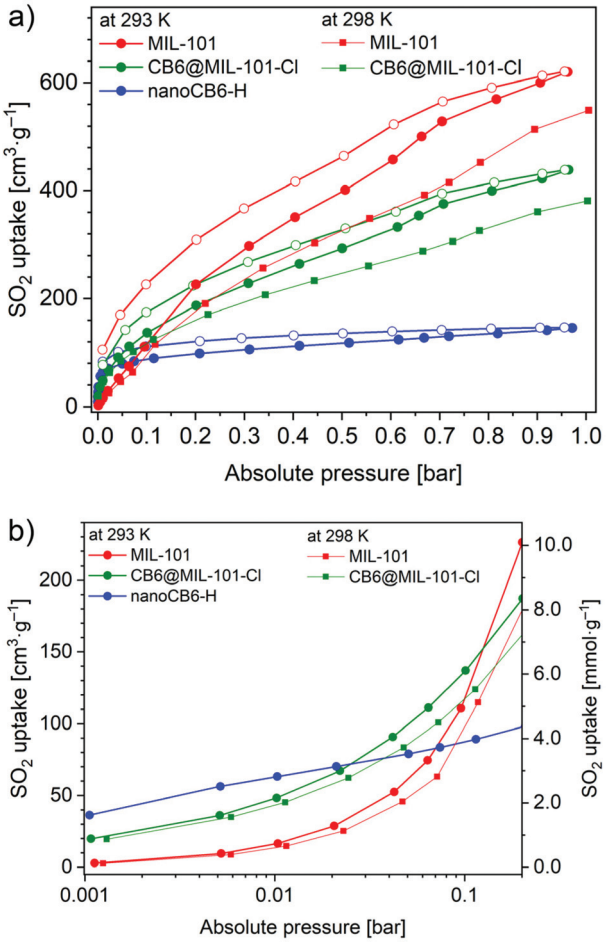

Fig. 2 SO_2 sorption isotherms for MIL-101 and CB6@MIL-101-Cl at 293 K (normal lines) and 298 K (thin lines, adsorption branch only), and for nanoCB6-H at 293 K: (a) 0–1 bar range. (b) 0.001–0.2 range, logarithmic scale (in b the desorption isotherms are omitted for clarity).

be only 1.3 mmol g^{-1} at 0.01 bar, indicating a synergistic effect in the composite CB6@MIL-101-Cl. At 0.01 bar, the SO_2 uptake of CB6@MIL-101-Cl (2.2 mmol g^{-1} at 293 K and 2.0 mmol g^{-1} at 298 K) is significantly higher than that of most MOF sorbents in the literature (Fig. S8, Table S6, ESI†), and only lower than that of SIFSIX-2-Cu-i and MIL-160 (4.2 mmol g^{-1}),[28,29] SIFSIX-1-Cu (3.4 mmol g^{-1}),[28] DMOF-TM (3.8 mmol g^{-1}),[35] MFM-305 (3.3 mmol g^{-1}),[27] MFM-305-CH_3, NH_2-MIL-125(Ti) and mmen-MIL-101(Cr) (3.0 mmol g^{-1}),[27,29,61] as well as SIFSIX-3-Ni (2.4 mmol g^{-1}).[28] However, those materials show a lower uptake at 1 bar compared to CB6@MIL-101-Cl (Table S6, ESI†).

The isosteric enthalpy of adsorption (ΔH_{ads}) for SO_2 adsorption on CB6@MIL-101-Cl and MIL-101 was calculated from the adsorption isotherms measured at 273 K and 293 K using the virial method (Fig. 3, Fig. S9 and S10, ESI†).[62] The near zero-coverage adsorption enthalpy of SO_2 (ΔH^0_{ads}) for CB6@MIL-101-Cl is ~–50 kJ mol^{-1}, while for MIL-101 it is ~–35 kJ mol^{-1}. The higher negative ΔH^0_{ads} of SO_2 for CB6@MIL-101-Cl proves that the incorporation of CB6 cages can indeed increase the affinity of materials towards SO_2, probably by narrowing the pores towards multiple optimal gas-adsorbent interactions[25,33,35,63] and providing intra/outer surfaces of the relatively polar CB6 for SO_2 adsorption, even if the loading may block some of the external sites.

It should be noted that the ΔH^0_{ads} value of SO_2 for nanoCB6-H was ~–76 kJ mol^{-1} when the material was activated at 150 °C, at the same temperature as CB6@MIL-101-Cl and MIL-101 (in previous work,[41] where nanoCB6-H was only activated at 100 °C, $\Delta H^0_{ads} = -65\ kJ\ mol^{-1}$ was given). From DFT-D3 (dispersion-corrected DFT) calculations on the possible binding sites for SO_2 at CB6 macrocycles the cavity of the CB6 cage was the highest-energy binding site with a calculated binding energy of −82 kJ mol^{-1}. There, SO_2 molecules are primarily adsorbed through two electrostatic $O_2S^{\delta+}\cdots^{\delta-}O{=}C$(CB6) interactions at an S···O distance of 3.04 Å. The intrinsic pore of CB6 is large enough (5.8 Å center diameter, 3.9 Å window diameters, 9.1 Å height) to encapsulate two SO_2 molecules, which can enter in these $O_2S^{\delta+}\cdots^{\delta-}O{=}C$(CB6) interactions in the confined space.[41] The second highest-energy binding site with calculated −50 kJ mol^{-1} has SO_2 located around the outer surface and involves electrostatic $O_2S^{\delta+}\cdots^{\delta-}O{=}C$(CB6), $O_2S^{\delta+}\cdots^{\delta-}N$(CB6) and $OSO^{\delta-}\cdots^{\delta+}H$–C(CB6) interactions.[41]

With regard to ΔH^0_{ads}, the composite is closer to MIL-101 than to nanoCB6-H, while in the case of a non-interacting, physical mixture, ΔH^0_{ads} should be equal to the latter. The decrease could be interpreted as a blockage of active sites, *e.g. via* MIL-host···CB6-guest interactions. Also, the state of the CB6 guests in the MIL pores will be rather amorphous; thereby, the high values for the CB6-H crystalline state, could barely be expected. With increased loading of SO_2, the isosteric enthalpy of adsorption ($-\Delta H_{ads}$) of all three materials is decreased (Fig. 3), according to the occupation of binding sites in the order of decreasing binding energies, also indicating adsorbents with different sites.

Comparative FT-IR spectroscopy was employed to assess the possible SO_2 adsorption sites in CB6@MIL-101-Cl and MIL-101. A series of spectra of the SO_2 loaded compounds with gradually decreasing SO_2 content, as a result of contact with ambient atmosphere (0 to 10 min), were collected as described in the Experimental section, and compared with the spectrum of the activated compound (Fig. 4). The new bands, appearing as a result of adsorption, at 1328 and 1144 cm^{-1} in CB6@MIL-101-Cl and at 1332 and 1146 cm^{-1} in MIL-101 are assigned to the asymmetric and symmetric stretching vibrations of the physisorbed SO_2 molecules.[64,65] The new bands are slightly shifted compared to the bands at 1330 and 1149 cm^{-1} for free SO_2 molecules, thereby indicating the interaction with the surface of the materials. The intensity of the bands assigned to the adsorbed SO_2 gradually decreases with time. The bands are traceable for around 2 minutes for MIL-101 and around 5 minutes for CB6@MIL-101-Cl under the same experimental conditions (Fig. 4, Fig. S11, ESI†). This can be seen in line with the difference in isosteric adsorption enthalpy since the adsorption kinetics are judged as similar from the similar hysteresis widths of the desorption isotherms for MIL-101 and CB6@MIL-101-Cl.

The comparison of the FT-IR spectra of the activated materials and the materials with variable SO_2 contents also show vibrational changes of functional groups of the frameworks. The bands at 1630 cm^{-1} and 1398 cm^{-1} in MIL-101 and at 1632 cm^{-1} and 1394 cm^{-1} in CB6@MIL-101-Cl are attributed to the asymmetric ν_{as} and symmetric ν_s carboxylate (COO) stretching vibrations.[61,66] In both materials, after exposed once to SO_2, the carboxylate ν_{as}(COO) band is red-shifted (Δ = −3 cm^{-1}), and the ν_s(COO) band is blue-shifted (Δ = 5 cm^{-1} for CB6@MIL-101-Cl and invariant within experimental error of ±2 cm^{-1} for MIL-101).

It is worth nothing that the carboxylate frequency shifts observed for CB6@MIL-101-Cl tend to be more pronounced compared to MIL-101. Additionally, the IR spectral response of

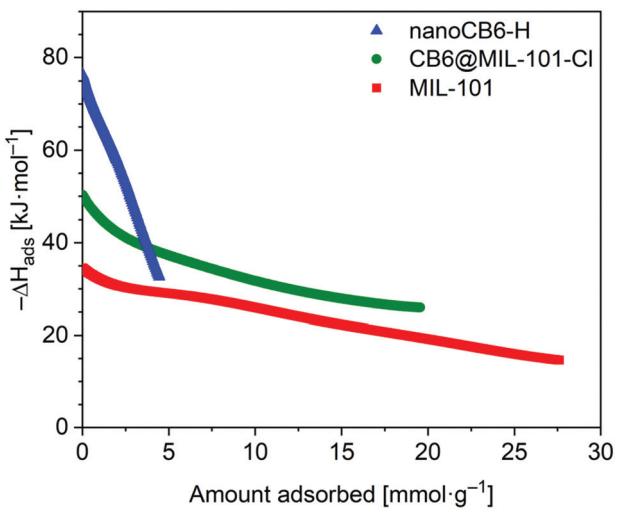

Fig. 3 Isosteric enthalpy of adsorption dependence on the amount of SO_2 adsorbed for MIL-101, CB6@MIL-101-Cl and nanoCB6-H.

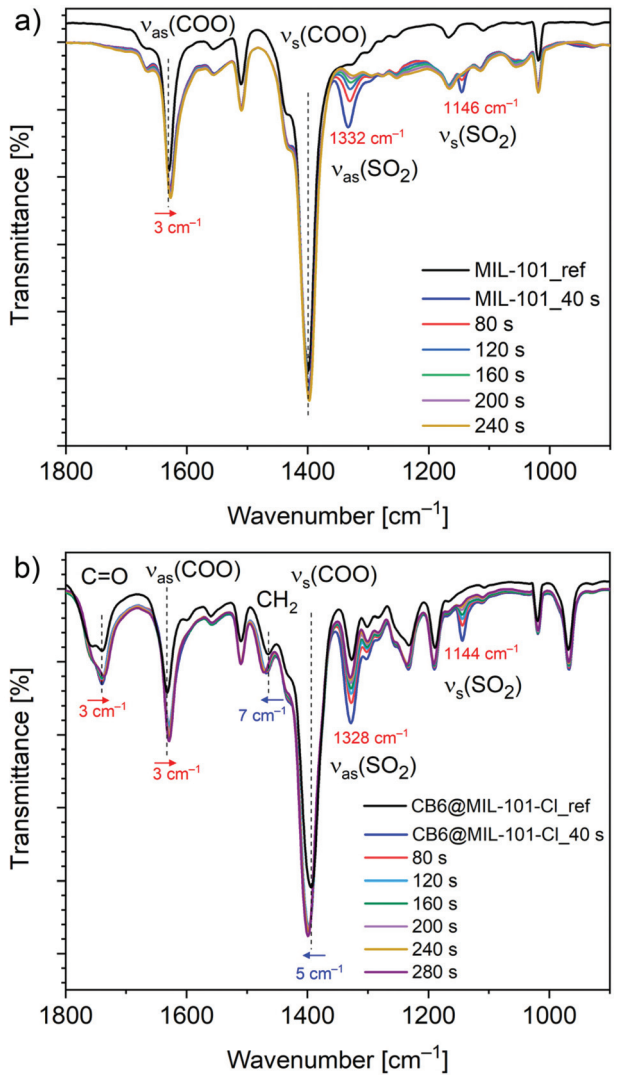

Fig. 4 FT-IR spectra of (a) MIL-101 and (b) CB6@MIL-101-Cl before and after single exposure and loading with SO_2 (see Exp. section for details).

CB6 in CB6@MIL-101-Cl upon SO_2 exposure is also clearly traceable. Thus, the carbonyl stretching vibration ν(CO) = 1740 cm^{-1} of CB6 demonstrates a red shift (Δ = −3 cm^{-1}) upon SO_2 adsorption and the methylene bending vibration $\nu(CH_2)$ = 1465 cm^{-1} a blue shift (Δ = 7 cm^{-1}) indicating interactions between SO_2 and CB6. In comparison, nanoCB6-H under the same conditions on the same instrument features a slightly stronger red shift of ν(CO) (Δ = −6 cm^{-1}) and a slightly weaker blue shift of $\nu(CH_2)$ (Δ = 4 cm^{-1}).[41]

The FT-IR spectra (Fig. S12, ESI†) of MIL-101 and CB6@MIL-101-Cl after one full SO_2 ad/desorption cycle followed by degassing at 150 °C and 1 × 10^{-3} mbar for 12 h were also measured. It was found that the spectrum of CB6@MIL-101-Cl was essentially unchanged within experimental error which supports the stability of CB6@MIL-101-Cl towards dry SO_2 sorption. In MIL-101, the broad ν_{as}(COO) band in MIL-101, initially at ~1630 cm^{-1}, is remarkably red-shifted (Δ = −10 cm^{-1}). The shift is comparable to the one observed in SO_2 loaded MFM-170 carboxylate MOF (Δ = −10 cm^{-1}), suggesting the interaction between SO_2 and carboxylate groups in the framework.[24] More importantly, new bands at 1100 cm^{-1} and 1049 cm^{-1} and a broad band at 900–1200 cm^{-1} appeared, which were attributed to the presence of sulfite and hydrogensulfite species.[64,67,68] This is in line with the observation from XPS (Fig. S5, Table S4, ESI†). The broadening of the ν_{as}(COO) band indicates the partial collapse and decrease of the local uniformity in the MIL-101 framework.

To further investigate the stability of these materials against dry SO_2, we performed cyclic adsorption–desorption at 293 K up to 0.96 bar for three runs for MIL-101, MIL-101-Cl and CB6@MIL-101-Cl and also for 10 runs for CB6@MIL-101-Cl (see the Experimental section). The uptake by MIL-101 gradually decreased to 40% from 620 to 245 cm^3 g^{-1} (Fig. S13, ESI†), as expected from earlier reports,[61,69] while CB6@MIL-101-Cl maintained 95% of the initial uptake amount also over 10 cycles (Fig. 5). It is worth noting here that statements about the limited stability of MIL-101 against dry SO_2 can be found in a few publications.[31,61] Ibarra *et al.* had noted that not only the chromium-hydroxide-containing MIL-101, *i.e.* [Cr$_3$(O)(OH)(H$_2$O)$_2$(BDC)$_3$], but also the more crystalline chromium-fluoride-containing MIL-101 compound, *i.e.* [Cr$_3$(O)F(H$_2$O)$_2$(BDC)$_3$], were unstable (*cf.* sample MIL-101(Cr)-HF, Fig. S22–S24 in the ESI of ref. 31†). A MIL-101 with stability towards dry and humid SO_2 could only be obtained with partial incorporation of a fully fluorinated BDC ligand, giving the sample MIL-101(Cr)-4F(1%) which then showed a high SO_2 uptake capacity of 18.4 mmol g^{-1} at 1 bar and 298 K.[31] There is an ambiguity regarding the scattered literature data on the stability of Cr(III)-MOFs, but the instability against dry SO_2 is the more surprising as Cr(III)-MOFs are in general considered to be highly kinetically inert.

The enhanced stability of the CB6@MIL-101-Cl composite towards dry SO_2 could be explained by the hydroxido-to-chlorido ligand exchange, that is the substitution of the terminal

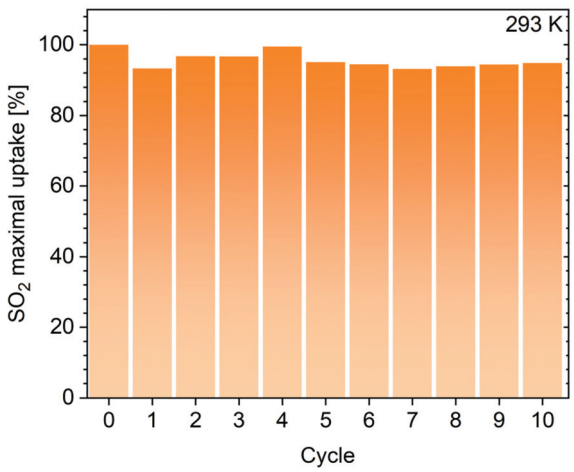

Fig. 5 SO_2 adsorption capacity of CB6@MIL-101-Cl at 293 K and 0.96 bar, measured over 10 repetitive adsorption–desorption cycles.

Cr–OH ligand in the $[Cr_3(O)X(H_2O)_2(BDC)_3]$ coordination framework of MIL-101 by Cr–Cl in CB6@MIL-101-Cl. To check the hypothesis a sample of MIL-101-Cl was prepared from MIL-101 in the absence of CB6 but otherwise under the same conditions as CB6@MIL-101-Cl, and submitted to SO_2 adsorption–desorption cycling for three runs (Fig. S13, ESI†). The textural properties of MIL-101-Cl are listed in Table S7, ESI.† The BET surface area of MIL-101-Cl is somewhat higher than that of the parent MIL-101, which we reason with the decomposition of pore-filling residual coordination species by HCl and the subsequent removal through the washing processes.[70] MIL-101-Cl have kept 97% adsorption capacity of the initial uptake after three adsorption–desorption runs at 293 K (Fig. S13, ESI†). The N_2 sorption-based BET-surface area and total pore volume of MIL-101, CB6@MIL-101-Cl and MIL-101-Cl before and after multi-cycle SO_2 sorption confirmed the above conclusions from the cyclic SO_2 sorption experiments. The BET surface area decreased by 45% (1768 $m^2\ g^{-1}$ *vs.* 3217 $m^2\ g^{-1}$) for MIL-101, but was retained within experimental error (2036 $m^2\ g^{-1}$ *vs.* 2077 $m^2\ g^{-1}$) for CB6@MIL-101-Cl and even slightly increased (3541 $m^2\ g^{-1}$ *vs.* 3408 $m^2\ g^{-1}$) for MIL-101-Cl after exposure to SO_2 at 293 K (Table S7, ESI†). The comparison of the PXRD patterns before and after cyclic SO_2 sorption for MIL-101, CB6@MIL-101-Cl and MIL-101-Cl verified the preservation of the crystallinity in the two later cases compared to the deterioration of the parent material MIL-101 (Fig. S14, ESI†). Thereby, the combined N_2 adsorption and PXRD data confirm the enhanced stability of CB6@MIL-101-Cl and MIL-101-Cl against SO_2 compared to the instability of the parent MIL-101. Further, the comparative experiments with MIL-101-Cl suggest that its increased stability is due to the facile one-step hydroxido-to-chlorido ligand exchange in the framework.

In this work we are focusing on the enhanced SO_2 uptake and stability of CB6@MIL-101-Cl. The interesting and counterintuitive instability of the parent MIL-101 will be thoroughly addressed in a follow-up study.

Considering the inevitable moisture presence for any possible real-world applications, the stability of materials towards humid SO_2 was also investigated by PXRD diffraction and N_2 sorption analyses. The PXRD patterns of MIL-101 and CB6@MIL-101-Cl after humid SO_2 treatment were retained, indicating their intact frameworks. In contrast, nanoCB6-H lost most of its crystallinity under acidic humid SO_2 atmosphere condition. (Fig. S15, ESI†). N_2 adsorption–desorption isotherms (Fig. 6) showed that MIL-101 and CB6@MIL-101-Cl kept the BET surface areas unchanged after exposure to humid SO_2 (35 ppm) for 6 h.

The BET surface area of nanoCB6-H significantly decreased and only 18% of the initial BET surface area was retained (Table S7, ESI†). This result confirmed again that the hydrogen-bonded organic framework nanoCB6-H is unstable in humid conditions, which is in line with our previous study.[41] The fact that MIL-101 was unstable in dry SO_2 but stable in humid SO_2 conditions could be related to the role of water vapor. We propose that under dry conditions, the Cr-OH site of MIL-101 is

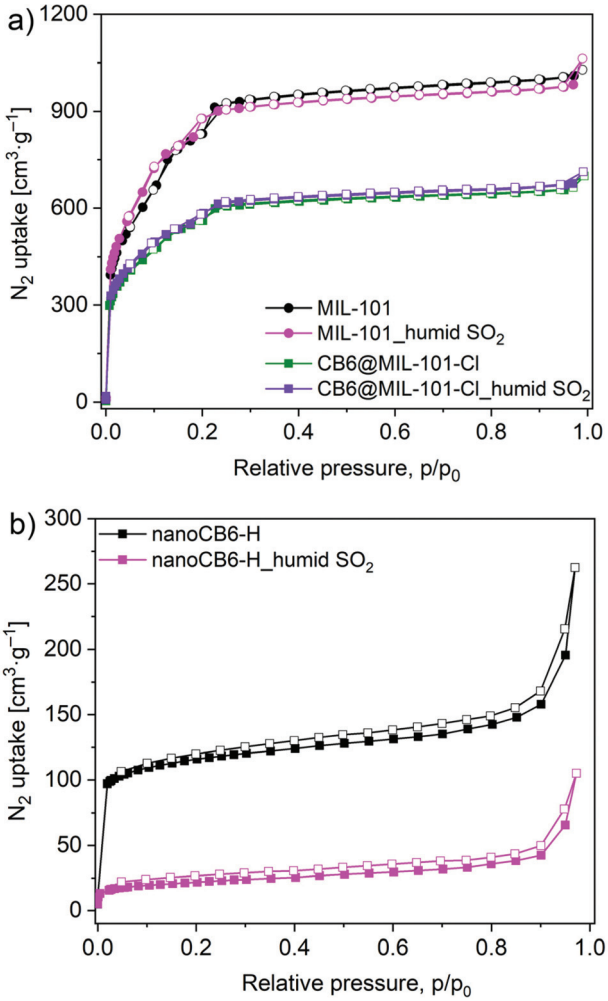

Fig. 6 N_2 adsorption isotherms (77 K) for (a) MIL-101 and CB6@MIL-101-Cl; (b) nanoCB6-H after exposure to humid SO_2 for 6 h.

well accessible for the reaction with SO_2 molecules, while under humid conditions this site (and possibly other reactive sites) is blocked and protected by water clusters. Note that MIL-101 has a medium hydrophilic surface and good stability in acidic solution.[71–73] A similar counterintuitive observation was made in Zeolite Y, which exhibited a better stability performance under humid SO_2 exposure conditions than toward dry SO_2. Also for Zeolite Y the pre-adsorbed water in this highly hydrophilic framework may block the accessibility of SO_2.[25]

In addition, the full SO_2 sorption isotherms of these three samples (MIL-101, CB6@MIL-101-Cl and nanoCB6-H) after exposure to humid SO_2 (35 ppm) for 6 h were measured (Fig. S16, ESI†). The SO_2 uptake capacity of nanoCB6-H after exposure to humid SO_2 decreased due to its decreased porosity (Fig. 7). Both MIL-101 and CB6@MIL-101-Cl showed unchanged or even slightly increased SO_2 uptakes at 0.01 bar together with around 20% loss of total uptake capacity at 1 bar when compared to dry SO_2 sorption (Fig. 7, Table S8, ESI†). Therefore, CB6@MIL-101-Cl exhibits enhanced stability and SO_2 removal capability over MIL-101 under lower press-

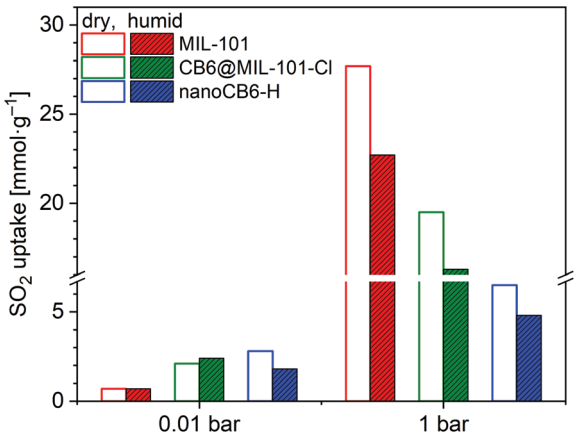

Fig. 7 SO_2 adsorption uptake (293 K) for MIL-101, CB6@MIL-101-Cl and nanoCB6-H after exposure to humid SO_2 for 6 h compared to the behavior under dry conditions (Table S8, ESI†).

ures in both dry SO_2 and humid conditions. This stability under humid conditions is a necessity for realistic applications in view of the ubiquitous presence of water.

Conclusions

We have systematically investigated a cage/MOF composite, named CB6@MIL-101-Cl, obtained by wet impregnation of cucurbituril, CB6 cages into the pores of MIL-101 for potential SO_2 gas removal. It is found that CB6@MIL-101-Cl shows enhanced performance in the removal of SO_2 gas under low pressure due to the combined merits of CB6 cages with high affinity towards SO_2 and MIL-101 with hierarchical pores. The relatively strong interactions between SO_2 molecules and CB6@MIL-101-Cl surfaces were supported by time-dependent FT-IR (ATR) spectra. MIL-101 was again confirmed to be unstable towards dry SO_2. The stability of CB6@MIL-101-Cl was enhanced when compared with MIL-101 due to the unexpected hydroxido-to-chloride exchange in the $\{Cr_3(O)X(BDC)_3\}$ metal node of MIL-101. This unexpected postsynthetic modification was supported by EDX and XPS analysis of related materials. The targeted CB6@MIL-101-Cl shows a high SO_2 uptake of 19.5 mmol g^{-1} at 293 K and 1 bar and high chemical stability even under humid SO_2 conditions. The counterintuitive instability of the parent MIL-101 and the observed enhanced stability of MIL-101-Cl is an unexpected finding, which will be thoroughly addressed in a follow-up study and for which the technological importance might be very high. The investigation of the comparable stabilities of different MIL-101-X materials, where X is a terminal counter-anion, is a task, which we are targeting in the near future.

Conflicts of interest

There are no conflicts to declare.

Author contributions

All the authors have significantly contributed to the paper and have given approval to the final version of the manuscript.

Acknowledgements

We thank the China Scholarship Council (CSC) for granting a Ph.D. fellowship to Y. Y. S. J. L. acknowledges financial support of NSFC (22001178) and support from the Hoffmann Institute of Advanced Materials (HIAM), Shenzhen Polytechnic. The authors thank Dr István Boldog, Dr Shanghua Xing, Mr Dennis Woschko and Mrs. Stefanie Bügel for helpful assistance and discussion.

References

1 Z. Klimont, S. Smith and J. Cofala, *Environ. Res. Lett.*, 2013, **8**, 014003.
2 X. Xu, C. Chen, H. Qi, R. He, C. You and G. Xiang, *Fuel Process. Technol.*, 2000, **62**, 153–160.
3 P. Amoatey, H. Omidvarborna, M. S. Baawain and A. Al-Mamun, *Process Saf. Environ. Prot.*, 2019, **123**, 215–228.
4 M. Matooane and R. Diab, *Arch. Environ. Health*, 2003, **58**, 763–770.
5 F. C. Menz and H. M. Seip, *Environ. Sci. Policy*, 2004, **7**, 253–265.
6 J. Yang, L. Li, S. Wang, H. Li, J. S. Francisco, X. C. Zeng and Y. Gao, *J. Am. Chem. Soc.*, 2019, **141**, 19312–19320.
7 B. Wu, H. Tian, Y. Hao, S. Liu, X. Liu, W. Liu, X. Bai, W. Liang, S. Lin, Y. Wu, P. Shao, H. Liu and C. Zhu, *Environ. Sci. Technol.*, 2018, **52**, 14015–14026.
8 R. K. Srivastava and W. Jozewicz, *J. Air Waste Manage. Assoc.*, 2001, **51**, 1676–1688.
9 J.-Y. Lee, T. C. Keener and Y. J. Yang, *J. Air Waste Manage. Assoc.*, 2009, **59**, 725–732.
10 R. K. Srivastava, W. Jozewicz and C. Singer, *Environ. Prog.*, 2001, **20**, 219–228.
11 A. B. Rao and E. S. Rubin, *Environ. Sci. Technol.*, 2002, **36**, 4467–4475.
12 R. Pacciani, J. Torres, P. Solsona, C. Coe, R. Quinn, J. Hufton, T. Golden and L. F. Vega, *Environ. Sci. Technol.*, 2011, **45**, 7083–7088.
13 M. P. Suh, H. J. Park, T. K. Prasad and D.-W. Lim, *Chem. Rev.*, 2012, **112**, 782–835.
14 J.-R. Li, R. J. Kuppler and H.-C. Zhou, *Chem. Soc. Rev.*, 2009, **38**, 1477–1504.
15 J.-R. Li, J. Sculley and H.-C. Zhou, *Chem. Rev.*, 2012, **112**, 869–932.
16 J. B. DeCoste and G. W. Peterson, *Chem. Rev.*, 2014, **114**, 5695–5727.
17 H. Wang, W. P. Lustig and J. Li, *Chem. Soc. Rev.*, 2018, **47**, 4729–4756.

18 E. Martínez-Ahumada, M. L. Díaz-Ramírez, M. d. J. Velásquez-Hernández, V. Jancik and I. A. Ibarra, *Chem. Sci.*, 2021, **12**, 6772–6799.
19 T. Islamoglu, Z. Chen, M. C. Wasson, C. T. Buru, K. O. Kirlikovali, U. Afrin, M. R. Mian and O. K. Farha, *Chem. Rev.*, 2020, **120**, 8130–8160.
20 K. Sumida, D. L. Rogow, J. A. Mason, T. M. McDonald, E. D. Bloch, Z. R. Herm, T.-H. Bae and J. R. Long, *Chem. Rev.*, 2012, **112**, 724–781.
21 W. P. Mounfield, C. Han, S. H. Pang, U. Tumuluri, Y. Jiao, S. Bhattacharyya, M. R. Dutzer, S. Nair, Z. Wu, R. P. Lively, D. S. Sholl and K. S. Walton, *J. Phys. Chem. C*, 2016, **120**, 27230–27240.
22 M. R. Tchalala, P. M. Bhatt, K. N. Chappanda, S. R. Tavares, K. Adil, Y. Belmabkhout, A. Shkurenko, A. Cadiau, N. Heymans, G. Weireld, G. Maurin, K. N. Salama and M. Eddaoudi, *Nat. Commun.*, 2019, **10**, 1328.
23 J. H. Carter, X. Han, F. Y. Moreau, I. da Silva, A. Nevin, H. G. W. Godfrey, C. C. Tang, S. Yang and M. Schröder, *J. Am. Chem. Soc.*, 2018, **140**, 15564–15567.
24 G. L. Smith, J. E. Eyley, X. Han, X. Zhang, J. Li, N. M. Jacques, H. G. W. Godfrey, S. P. Argent, L. J. McCormick McPherson, S. J. Teat, Y. Cheng, M. D. Frogley, G. Cinque, S. J. Day, C. C. Tang, T. L. Easun, S. Rudić, A. J. Ramirez-Cuesta, S. Yang and M. Schröder, *Nat. Mater.*, 2019, **18**, 1358–1365.
25 P. Brandt, A. Nuhnen, S. Öztürk, G. Kurt, J. Liang and C. Janiak, *Adv. Sustainable Syst.*, 2021, **5**, 2000285.
26 Y. Zhang, P. Zhang, W. Yu, J. Zhang, J. Huang, J. Wang, M. Xu, Q. Deng, Z. Zeng and S. Deng, *ACS Appl. Mater. Interfaces*, 2019, **11**, 10680–10688.
27 L. Li, I. da Silva, D. I. Kolokolov, X. Han, J. Li, G. Smith, Y. Cheng, L. L. Daemen, C. G. Morris, H. G. W. Godfrey, N. M. Jacques, X. Zhang, P. Manuel, M. D. Frogley, C. A. Murray, A. J. Ramirez-Cuesta, G. Cinque, C. C. Tang, A. G. Stepanov, S. Yang and M. Schröder, *Chem. Sci.*, 2019, **10**, 1472–1482.
28 X. Cui, Q. Yang, L. Yang, R. Krishna, Z. Zhang, Z. Bao, H. Wu, Q. Ren, W. Zhou, B. Chen and H. Xing, *Adv. Mater.*, 2017, **29**, 1606929.
29 P. Brandt, A. Nuhnen, M. Lange, J. Möllmer, O. Weingart and C. Janiak, *ACS Appl. Mater. Interfaces*, 2019, **11**, 17350–17358.
30 M. Savage, Y. Cheng, T. L. Easun, J. E. Eyley, S. P. Argent, M. R. Warren, W. Lewis, C. Murray, C. C. Tang, M. D. Frogley, G. Cinque, J. Sun, S. Rudić, R. T. Murden, M. J. Benham, A. N. Fitch, A. J. Blake, A. J. Ramirez-Cuesta, S. Yang and M. Schröder, *Adv. Mater.*, 2016, **28**, 8705–8711.
31 E. Martínez-Ahumada, M. L. Díaz-Ramírez, H. A. Lara-García, D. R. Williams, V. Martis, V. Jancik, E. Lima and I. A. Ibarra, *J. Mater. Chem. A*, 2020, **8**, 11515–11520.
32 Ü. Kökçam-Demir, A. Goldman, L. Esrafili, M. Gharib, A. Morsali, O. Weingart and C. Janiak, *Chem. Soc. Rev.*, 2020, **49**, 2751–2798.
33 P. Brandt, S.-H. Xing, J. Liang, G. Kurt, A. Nuhnen, O. Weingart and C. Janiak, *ACS Appl. Mater. Interfaces*, 2021, **13**, 29137–29149.
34 F. Chen, D. Lai, L. Guo, J. Wang, P. Zhang, K. Wu, Z. Zhang, Q. Yang, Y. Yang, B. Chen, Q. Ren and Z. Bao, *J. Am. Chem. Soc.*, 2021, **143**, 9040–9047.
35 S. Xing, J. Liang, P. Brandt, F. Schäfer, A. Nuhnen, T. Heinen, I. Boldog, J. Möllmer, M. Lange, O. Weingart and C. Janiak, *Angew. Chem., Int. Ed.*, 2021, **60**, 17998–18005.
36 Y. Lin, H. Lin, H. Wang, Y. Suo, B. Li, C. Kong and L. Chen, *J. Mater. Chem. A*, 2014, **2**, 14658–14665.
37 F. P. Kinik, A. Uzun and S. Keskin, *ChemSusChem*, 2017, **10**, 2842–2863.
38 I. Cota and F. Fernandez Martinez, *Coord. Chem. Rev.*, 2017, **351**, 189–204.
39 D. K. Yoo, N. Abedin Khan and S. H. Jhung, *J. CO_2 Util.*, 2018, **28**, 319–325.
40 Q.-X. Luo, B.-W. An, M. Ji and J. Zhang, *Mater. Chem. Front.*, 2018, **2**, 219–234.
41 J. Liang, S. Xing, P. Brandt, A. Nuhnen, C. Schlüsener, Y. Sun and C. Janiak, *J. Mater. Chem. A*, 2020, **8**, 19799–19804.
42 S. Lim, H. Kim, N. Selvapalam, K.-J. Kim, S. J. Cho, G. Seo and K. Kim, *Angew. Chem., Int. Ed.*, 2008, **47**, 3352–3355.
43 J. Tian, J. Liu, J. Liu and P. K. Thallapally, *CrystEngComm*, 2013, **15**, 1528–1531.
44 J. Liang, A. Nuhnen, S. Millan, H. Breitzke, V. Gvilava, G. Buntkowsky and C. Janiak, *Angew. Chem., Int. Ed.*, 2020, **59**, 6068–6073.
45 *Match! – phase analysis using powder diffraction, 2019 (v.3.5.3.109), H. Putz – Crystal Impact GbR*, 53227 Bonn, Germany.
46 T. Zhao, F. Jeremias, I. Boldog, B. Nguyen, S. K. Henninger and C. Janiak, *Dalton Trans.*, 2015, **44**, 16791–16801.
47 G. Férey, C. Mellot-Draznieks, C. Serre, F. Millange, J. Dutour, S. Surblé and I. Margiolaki, *Science*, 2005, **309**, 2040.
48 G. Férey, C. Mellot-Draznieks, C. Serre and F. Millange, *Acc. Chem. Res.*, 2005, **38**, 217–225.
49 J. Liang, Y.-Q. Xie, X.-S. Wang, Q. Wang, T.-T. Liu, Y.-B. Huang and R. Cao, *Chem. Commun.*, 2018, **54**, 342–345.
50 O. Buyukcakir, S. H. Je, S. N. Talapaneni, D. Kim and A. Coskun, *ACS Appl. Mater. Interfaces*, 2017, **9**, 7209–7216.
51 S. M. Towsif Abtab, D. Alezi, P. M. Bhatt, A. Shkurenko, Y. Belmabkhout, H. Aggarwal, Ł. J. Weseliński, N. Alsadun, U. Samin, M. N. Hedhili and M. Eddaoudi, *Chem*, 2018, **4**, 94–105.
52 Y. Shen, T. Pan, P. Wu, J. Huang, H. Li, I. E. Khalil, S. Li, B. Zheng, J. Wu, Q. Wang, W. Zhang, D. Wei Wei and F. Huo, *CCS Chem.*, 2020, **2**, 1607–1614.
53 X. Huang, Q. Hu, L. Gao, Q. Hao, P. Wang and D. Qin, *RSC Adv.*, 2018, **8**, 27623–27630.
54 M. Saikia and L. Saikia, *RSC Adv.*, 2016, **6**, 14937–14947.
55 F. Zhang, Y. Jin, Y. Fu, Y. Zhong, W. Zhu, A. A. Ibrahim and M. S. El-Shall, *J. Mater. Chem. A*, 2015, **3**, 17008–17015.
56 S. H. Overbury, D. R. Mullins, D. R. Huntley and L. Kundakovic, *J. Phys. Chem. B*, 1999, **103**, 11308–11317.

57 E. J. Romano and K. H. Schulz, *Appl. Surf. Sci.*, 2005, **246**, 262–270.
58 H. C. Yoon, P. B. S. Rallapalli, H. T. Beum, S. S. Han and J.-N. Kim, *Energy Fuels*, 2018, **32**, 1365–1373.
59 H. B. Tanh Jeazet, C. Staudt and C. Janiak, *Chem. Commun.*, 2012, **48**, 2140–2142.
60 M. Thommes, K. Kaneko, A. V. Neimark, J. P. Olivier, F. Rodriguez-Reinoso, J. Rouquerol and S. W. Sing, *Pure Appl. Chem.*, 2015, **87**, 1051–1069.
61 Z. Zhang, B. Yang and H. Ma, *Sep. Purif. Technol.*, 2021, **259**, 118164.
62 A. Nuhnen and C. Janiak, *Dalton Trans.*, 2020, **49**, 10295–10307.
63 A. M. Ebrahim, B. Levasseur and T. J. Bandosz, *Langmuir*, 2013, **29**, 168–174.
64 A. L. Goodman, P. Li, C. R. Usher and V. H. Grassian, *J. Phys. Chem. A*, 2001, **105**, 6109–6120.
65 K. Tan, P. Canepa, Q. Gong, J. Liu, D. H. Johnson, A. Dyevoich, P. K. Thallapally, T. Thonhauser, J. Li and Y. J. Chabal, *Chem. Mater.*, 2013, **25**, 4653–4662.
66 Z. Zhou, B. Cheng, C. Ma, F. Xu, J. Xiao, Q. Xia and Z. Li, *RSC Adv.*, 2015, **5**, 94276–94282.
67 M. Waqif, A. M. Saad, M. Bensitel, J. Bachelier, O. Saur and J.-C. Lavalley, *J. Chem. Soc., Faraday Trans.*, 1992, **88**, 2931–2936.
68 W. P. Mounfield, U. Tumuluri, Y. Jiao, M. Li, S. Dai, Z. Wu and K. S. Walton, *Microporous Mesoporous Mater.*, 2016, **227**, 65–75.
69 N. Tannert, Y. Sun, E. Hastürk, S. Nießing and C. Janiak, *Z. Anorg. Allg. Chem.*, 2021, **647**, 1124–1130.
70 K. Wang, D. Feng, T.-F. Liu, J. Su, S. Yuan, Y.-P. Chen, M. Bosch, X. Zou and H.-C. Zhou, *J. Am. Chem. Soc.*, 2014, **136**, 13983–13986.
71 K. Leus, T. Bogaerts, J. De Decker, H. Depauw, K. Hendrickx, H. Vrielinck, V. Van Speybroeck and P. Van Der Voort, *Microporous Mesoporous Mater.*, 2016, **226**, 110–116.
72 J. Canivet, A. Fateeva, Y. Guo, B. Coasne and D. Farrusseng, *Chem. Soc. Rev.*, 2014, **43**, 5594–5617.
73 A. Khutia, H. U. Rammelberg, T. Schmidt, S. Henninger and C. Janiak, *Chem. Mater.*, 2013, **25**, 790–798.